Geology of Ore Deposits, Vol. 45, No. 2, 2003, pp. 133–150. Translated from Geologiya Rudnykh Mestorozhdenii, Vol. 45, No. 2, 2003, pp. 152–171.

Crystal Chemistry, Stability, and Formation Conditions of Sulfides with Sphalerite-Like Crystal Structures

N. S. Bortnikov[1] and T. L. Evstigneeva

Institute of Geology of Ore Deposits, Petrography, Mineralogy, and Geochemistry, Russian Academy of Sciences, Staromonetnyi per. 35, Moscow, 119017 Russia

Received December 30, 2002

Abstract—Compositional and structural characteristics of ore minerals were studied in detail using a combination of physical and chemical methods with wide application of modern equipment and sophisticated programs for data processing. A comprehensive analysis of types of inclusions in chalcopyrite and possible mechanisms of their formation was conducted on the example of the sphalerite–chalcopyrite system. It was shown that regular intergrowths do not prove high-temperature genesis but could be formed under specific crystallization rates and composition of the hydrothermal solution. The valence state and coordination of atoms were studied in the structures of stannite-group compounds. It was found that iron substitutes for copper and zinc in the isomorphic series kuramite–stannite (Cu_3SnS_4–Cu_2FeSnS_4) and kesterite–stannite (Cu_2ZnSnS_4–$CuFeSnS_4$), filling octahedral voids and forming tetrahedral vacancies in the closest packing of sulfur atoms. It was demonstrated by Mössbauer analysis that iron occurs in both di- and trivalent states in the two series. There is a limiting concentration of Fe atoms, Fe(x) ≈ 0.5, below which all iron is ferric and octahedrally coordinated by S atoms. Also considered were the reasons for difficulties in the application of regularities in the partitioning of elements and stable isotopes between coexisting minerals (on the example of sphalerite and stannite). Temperatures calculated by various geothermometers were compared, and an explanation was proposed for the observed discrepancy. The investigation of isomorphism in ore systems indicated the block structure of mineral segregations and their synthetic analogues. The compositional heterogeneity of ore minerals is mostly caused by the presence of tiny inclusions of a second phase or of intergrowths on micro- and submicro- (nano-) levels. The achievements of nanomineralogy, a rapidly developing branch of mineralogy, demonstrate that one of the major reasons for the observed deviations from the expected behavior of minerals and their aggregates is the size factor.

INTRODUCTION

Sulfides are carriers of many metals and often compose geologic bodies of considerable volumes. The investigation of factors controlling sulfide stability is important for the elucidation of genetic characteristics of ore deposits. In recent years, considerable attention has been directed toward the search for dependencies between the parameters of the crystal structure and chemical composition of sulfides and the conditions of their formation. Many sulfides were experimentally synthesized, and their stability fields were outlined. This provided insights into many problems of the conditions of ore formation in nature. At the same time, the new data require revision of existing concepts on the origin of diverse intergrowths of ore minerals.

Of course, the results of experimental studies cannot answer many questions concerning the formation of ore deposits. This is related to the fact that natural processes are much more complicated than the reactions that are reproduced in laboratories. Moreover, the parameters of precipitation of sulfides, their stability, and types of isomorphism are not only controlled by equilibrium conditions in the environment.

The investigation of natural sulfides is complicated primarily by the compositional heterogeneity of minerals. This concerns mainly the problems of isomorphic substitutions in sulfides and uncertainty in the position of admixture components in their crystal structures. The investigation of the chemistry of a mineral often gives rise to the question whether a particular element is isomorphic in sulfides or occurs as inclusions of another mineral. Of equal importance is the understanding of the distribution of atoms of a trace element in the structure, which is related to crystal structure ordering, in turn responsible for structural transformations. Solution of these problems depends to a large extent on the level of analytical facilities a variable. A combination of modern methods (Raman spectroscopy, Mössbauer spectroscopy, photoelectron spectroscopy, etc.) allows determination of the valence state and coordination of atoms in a compound. The extensive application of modern electron microscopes with energy-dispersive detectors in mineralogical studies provides opportunities to determine the composition and structure of minerals in individual particles of the size of fractions of a micrometer. Particular emphasis in the investigation of the crystal chemistry of sulfides is given to the determination of crystal structures from

[1]Corresponding author: N.S. Bortnikov. e-mail: bns@igem.ru

Table 1. Minerals of the stannite group

Name	Formula	Space group	*a*, Å	*b*, Å	*c*, Å	*Z*	Reference
Stannite	Cu_2FeSnS_4	$I\bar{4}2m$	5.449	5.449	10.757	2	Hall *et al.*, 1978
Kesterite	Cu_2ZnSnS_4	$I\bar{4}$	5.427	5.427	10.871	2	Orlova, 1958; Hall *et al.*, 1978; Kissin, 1989
Sakuraiite	$Cu_2Zn(In, Sn)S_4$	$I\bar{4}2m$	5.45	5.45	10.91	2	Chvileva *et al.*, 1988
Hocartite	Ag_2FeSnS_4	$I\bar{4}2m$	5.72	5.72	10.98	2	
Briartite	Cu_2FeGeS_4	$I\bar{4}2m$	5.32	5.32	10.51	2	
Cernyite	Cu_2CdSnS_4	$I\bar{4}2m$	5.487	5.487	10.848	2	Szymanski, 1978
Velikite	Cu_2HgSnS_4	$I\bar{4}$	5.5749	5.5749	10.882	2	Evstigneeva and Kabalov, 1998
Kuramite	Cu_2CuSnS_4	$I\bar{4}2m$ ($I\bar{4}$)	5.445	5.445	10.75	2	Kovalenker *et al*., 1979

powdered samples by the methods of profile analysis. The data obtained in recent years indicate that existing concepts on isomorphism in sulfides, for instance, direct substitution of iron for copper, must be revised.

In this paper, we summarized some results obtained over many years on the characteristics of isomorphism in synthetic and natural sulfides and their stability in natural environments. This concerns primarily minerals with sphalerite-like structures. It was of interest to us to show how current data on the stability of synthetic sulfide solid solutions can be applied for the interpretation of some mineral intergrowths, which have been widely used in the practice of investigations as geothermometers with a fixed point.

CRYSTAL CHEMISTRY OF SULFIDES WITH STRUCTURES DERIVED FROM THE SPHALERITE STRUCTURE

The structures of a great number of minerals are derived from the sphalerite structural type. Of particular importance among them are minerals of the stannite and chalcopyrite groups. The structures of these sulfides are based on the closest packing of sulfur atoms, a half of the tetrahedral voids of which is occupied by metal atoms (Sn, Cu, Fe, Zn, Ag, Cd, Hg, Ge, and so on). The diversity of structures is related to the occupancy of positions with metal atoms. When the metal : sulfur ratio is 1 : 1, metal atoms are distributed over half of the tetrahedral voids in the closest packing of sulfur. When metal : sulfur > 1 : 1, the additional metal atoms are incorporated in the second half of the tetrahedral voids or in octahedral voids.

The stannite group includes many common and characteristic minerals of massive sulfide, gold, copper–nickel, silver, and other ore deposits. They show a remarkable diversity of compositions with the general formula A_2BSnS_4, where *A* = Cu, Ag and *B* = Fe, Cu, Zn, Cd, Ge, Hg, and so on. Among minerals of this family are kuramite (Cu_3SnS_4), kesterite (Cu_2ZnSnS_4), hocartite (Ag_2FeSnS_4), velikite (Cu_2HgSnS_4), cernyite (Cu_2CdSnS_4), and others (Table 1). The majority of compounds of the stannite family are characterized by high isomorphic capacity (up to tens of weight percent). A typical isomorphic admixture is iron in kuramite (Cu_3SnS_4) (Kovalenker *et al.*, 1979) and kesterite (Cu_2ZnSnS_4) (Chvileva *et al.*, 1988).

The X-ray diffraction patterns of all minerals of the stannite group are virtually identical to those of stannite and differ slightly only in unit-cell parameters (Table 1). The structure of the mineral stannite belongs to the space group $I\bar{4}2m$; its tetragonal unit cell is doubled relative to that of ZnS [$a = 5.449$ Å, $c = 10.757$ (4) Å, and $Z = 2$]. Metal atoms occupy all tetrahedra of sulfur atoms pointing in the same direction in a cubic closest packing: Fe–2*a* (000), Sn–2*b* (1/2 1/2 0), Cu–4*d* (0 1/2 1/4), and S–8*i* (*xxz*, $x = 0.7551$, $z = 0.8702$) (Hall *et al.*, 1978).

The structures of stannite-group minerals are similar and are derived from the cubic structure of sphalerite. However, there are differences in cell symmetry, distribution of atoms in layers perpendicular to the fourfold axis, and degree of distortion of sulfur tetrahedra around atoms of tin (germanium and indium), copper (silver), and iron (zinc, cadmium, and mercury).

Only the structures of kesterite (Hall *et al.*, 1978) and cernyite (Szymanski, 1978) were determined by the single-crystal method. It turned out that they belong to space group $I\bar{4}$ and, in contrast to stannite, are characterized by the absence of diagonal mirror-symmetry planes.

Intergrowths of stannite and sphalerite are widespread in ore deposits. It is supposed that they were formed by unmixing of a high-temperature solid solution. Broad compositional variations in the stannite–sphalerite series were detected in the ores of the silver–base metal deposit Prognoz (Gamyanin *et al.*, 1999).

Stannite rarely occurs as small (up to 1–2 mm) individual grains in the ores of this deposit. It is usually intimately associated with sphalerite, in which it forms "flamelike" zones. These zones may be discontinuous when they are very thin (0.001–0.05 mm) or continuous. Stannite contains from 0.49 to 13.70 wt % Fe and from 0.21–13.83 wt % Zn. With respect to the Fe/(Zn + Fe) ratio, almost the complete stannite–kesterite series is represented. An alternation of zones of iron-rich and zinc-rich stannite varieties was found in sphalerite. Springer (1972) studied the pseudobinary join Cu_2FeSnS_4–Cu_2ZnSnS_4 and found a miscibility gap in it. The observed oscillatory zoning of minerals from the Prognoz deposit suggests that the continuity in the natural stannite–kesterite series is probably related to the crystallization of these minerals under dynamic conditions. Under conditions of fluid "supercooling," nonequilibrium deposition resulted in the formation of metastable phases intermediate between stannite and kesterite, and a subsequent tendency to fluid–crystal equilibrium promoted the precipitation of stannite, whose composition lay in the field of homogeneous solid solution.

The results of the investigation of the Cu_2ZnSnS_4–Cu_2FeSnS_4 system suggest the existence of two solid solutions in the kesterite–stannite join: one based on Cu_2ZnSnS_4 and one based on Cu_2FeSnS_4 (Springer, 1972; Osadchii and Sorokin, 1989; Kissin, 1978). There is an opinion (Kissin and Owens, 1989) that Cu_2FeSnS_4 is not stannite in this case, but structurally different ferrokesterite. It is often accepted that iron substitutes for zinc in the kesterite structure, because the divalent ions of iron and zinc are similar in size. The existence of the kuramite–stannite series (Cu_3SnS_4–Cu_2FeSnS_4), in which ferrous iron substitutes for divalent copper, was supposed on the basis of comparison of the compositions, X-ray diffraction patterns, and properties of kuramite and stannite. However, the question of the mechanism of isomorphic substitutions in the stannite–kesterite series has not been fully resolved (Bernardini *et al.*, 2000), because, despite their similar sizes, the electron structure of the ions Fe^{2+}, Zn^{2+}, and Cu^{2+} is different.

ISOMORPHISM IN STANNITE-FAMILY COMPOUNDS

The kuramite–stannite system and the minerals stannite (Mushiston deposit) and kesterite (Kester deposit) were selected for a detailed investigation. Eleven members of the kuramite–stannite series, $Cu_{3-x}Fe_xSnS_4$ at $0 < x < 1$, with an increment of x of about 0.1, were synthesized from pure elements in evacuated silica tubes (heating up to 1150°C, annealed at 400°C for 960 h, and quenched in ice-cold water) (Evstigneeva *et al.*, 2001_a). The compositions of the synthesized compounds (Table 2) display a negative correlation between the copper and iron contents in this series (Fig. 1).

Table 2. Compositions of synthetic phases in the system $Cu_{3-x}Fe_xSnS_4$, wt %

x	Cu	Fe	Sn	S	Σ
0.08	41.74	1.08	34.11	24.72	101.65
0.14	42.71	1.56	31.04	23.85	99.16
0.29	39.68	3.79	29.62	29.32	102.41
0.40	40.50	4.83	28.96	23.36	97.65
0.51	39.16	6.60	29.39	26.31	101.46
0.58	35.28	7.88	30.00	29.33	102.49
0.71	35.89	8.89	28.96	27.07	100.81
0.84	32.03	11.18	29.65	29.70	102.56
0.97	33.77	11.52	28.21	25.69	99.16
0.96	29.80	12.88	26.5	29.9	98.1

Note: Analyses were obtained on an MS-46 Cameca electron microprobe (Institute of Geology of Ore Deposits, Petrography, Mineralogy, and Geochemistry, Russian Academy of Sciences; analyst, G.N. Muravitskaya) at 20 kV and 10 nA, using $CuFeS_2$ (Cu, Fe), Sn_{met} (Sn), and FeS_2 (Fe) as standards.

The kesterite sample (provided by O. Stavrov) showed the following composition (average of 10 analyses, wt %): 28.79–28.98 Cu, 12.06–12.21 Zn, 2.28–2.21 Fe, 27.09–27.15 Sn, 28.96–28.29 S, and a total of 99.18–98.84; the mineral formula is $Cu_{2.00–2.03}(Zn_{0.81–0.83}Fe_{0.18})Sn_{1.00–1.03}S_{3.99–3.94}$.

The following methods were used for the determination of the valence state and coordination environment of atoms in mineral structures: electron microprobe analysis on MS-46 Cameca (Institute of Geology of Ore Deposits, Mineralogy, Petrography, and Geochemistry, Russian Academy of Sciences) and Camebax Microbeam (Institute of Volcanology, Far East Division, Russian Academy of Science) electron microprobes at 20 kV and 10 nA using $CuFeS_2$ (Cu, Fe), Sn_{met} (Sn), and FeS_2 (Fe) as standards; profile analysis

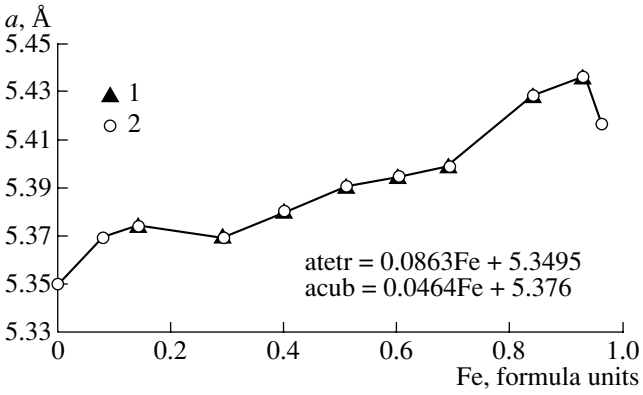

Fig. 1. Unit-cell parameters of compounds of the $Cu_{3-x}Fe_xSnS_4$ series: parameters of (1) tetragonal and (2) cubic (disordered) cells.

Table 3. Coordinates of metal atoms in the structures of $Cu_{3-x}Fe_xSnS_4$ compounds

Position	x = 0.29		x = 0.6		x = 0.84	
	Cu	Fe	Cu	Fe	Cu	Fe
2*a* (000)	0.82	0.08	0.72	0.28	1.0	0
2*c* (1/2 0 1/4)	1.0	0	0.80	0.16	0.76	0.24
2*d* (0 1/2 1/4)	0.94	0.09	1.0	0	0.60	0.40
2*b* (1/2 1/2 0)		0.12				0.10

(Rietveld method) on an ADP-2 diffractometer (CuK_α-radiation, Ni filter) with calculations by the WIRIET program (version 3.3); Mössbauer spectroscopy on an MS1001E mass spectrometer with a ^{57}Co source in a Rh matrix and ^{119}Sn in $BaSnO_3$ using the program package MSTools; scanning (JSM-5300 + Link ISIS) and transmission (JEM-100C + Kevex 5100 EDD) electron microscopy; and X-ray photoelectron spectroscopy (LAS-3000 Riber + OPX-150 semispherical photoelectron spectrometer, AlK_α radiation at 1486.6 eV, U = 12 kV, and I = 20 nA, calibrated by line 1*s* of carbon with a binding energy of 285 keV).

According to SEM and TEM data, all intermediate members of the kuramite–stannite series studied represented structurally similar homogeneous phases of a tetragonal space group showing regularly changing unit cell parameters ($c/a \sim 2$) (Table 1). The results of the structural analysis of four $Cu_{3-x}Fe_xSnS_4$ compounds with x = 0.3, 0.6, 0.8, and 1.0 revealed (Evstigneeva and Kabalov, 1998) that the first three of them are characterized by tetragonal structures, which, when compared with that of stannite (Cu_2FeSnS_4, $I\bar{4}2m$), have lower symmetry ($I\bar{4}$) and somewhat different distribution of metal atoms between the tetrahedral positions (Table 3). Attempts to substitute copper in various tetrahedral positions for iron in intermediate compounds of the kuramite–stannite series (especially at $x < 0.5$) failed despite good values of the R factor (3.4–3.8%): the R factor virtually did not change with increasing occupancy of the tetrahedral positions by iron (Evstigneeva *et al.*, 2001_1).

The synthetic end member Cu_2FeSnS_4 is a cubic modification of stannite with randomly distributed Fe^{2+}, Sn^{4+}, and Cu^{1+} (Evstigneeva and Kabalov, 2001). This is probably a synthetic analogue of "isostannite" (Ramdohr, 1975).

The experimental ^{57}Fe Mössbauer spectra of $Cu_{3-x}Fe_xSnS_4$ samples, including natural stannite from the Mushiston deposit, were recorded at room temperature. All of them are paramagnetic and, in general, superpositions of two partial spectra corresponding to ferrous and ferric iron (Fig. 2). In the $Cu_{3-x}Fe_xSnS_4$ samples with low iron content (up to x = 0.5), all iron occurs in the trivalent state. Trivalent iron ions are represented by a poorly resolved quadrupole doublet with isomer shift and quadrupole splitting values of δ = 0.35–0.40 mm/s and ε = 0.10–0.20 mm/s, respectively. The second partial spectrum appears in the spectra of $Cu_{3-x}Fe_xSnS_4$ with $x > 0.5$. It is a well-resolved quadrupole doublet with high quadrupole splitting, corresponding to Fe^{2+} (Fig. 2). The relative intensity of this doublet increases rapidly with increasing Fe concentration in the sample. The isomer shift and quadrupole splitting of this doublet vary within δ = 0.55–0.60 mm/s and ε = 0.8–1.4 mm/s, respectively (Evstigneeva *et al.*, 2003).

In all the phases studied, Sn exists in the tetravalent state in tetrahedral positions and shows a high degree of covalency of the Sn–S bonds (Evstigneeva *et al.*, 2001_1, 2001_2). With increasing concentration of iron, the degree of covalency of the Fe^{2+}–S and Sn^{4+}–S bonds decreases and that of Fe^{3+}–S increases. The effective charge of Sn in the tetrahedral positions of the structure is $Q_{Sn} = 3.38 \pm 0.08$ (Evstigneeva *et al.*, 2001_1).

The data of Mössbauer analysis explain why structure deciphering yielded no reliable result. The Rietveld refinement of the structure of the intermediate phase $Cu_{3-x}Fe_xSnS_4$ with $x \sim 0.6$ was carried out assuming iron in sixfold coordination (octahedra in the closest packing of sulfur atoms). The best fit (Rp = 2.69) was obtained for the occurrence of Fe^{3+} in the octahedral positions, which are unoccupied in the "normal" sphalerite structure [8*i* – *xxz* (xFe^{3+} ~ 1/4, zFe^{3+} ~ 0.126–0.128, zFe^{3+} = zS/3 + 5/12) zS = z atoms]. The distances $Me_{Oh} - Me_{Td}$ = 2.31–2.34 Å are comparable with the Me_{Td}–S distances, but lower than the distances for Me_{Oh}–S (2.57–2.81 Å) (Td and Oh denote the tetrahedral and octahedral positions, respectively).

In order to explain the unexpected results, two schemes of isomorphism were developed for the $Cu_{3-x}Fe_xSnS_4$ series (Evstigneeva *et al.*, 2001_1). At $0 < x < 0.5$, the process of substitution and changes in the structural and valence state of atoms proceeds with vacancy (□) formation via the scheme

$$2Cu^{2+}(Td) \longrightarrow Cu^{1+}(Td) + \square(Td) + Fe^{3+}(Oh),$$

and the formula of the transitional compounds is $Cu_2^{1+}Cu_{1-2x}^{2+}Fe_x^{3+}Cu_x^{1+}Sn^{4+}S_4$. The complete exhaustion of Cu^{2+} produces the end member $Cu_{2.5}^{1+}Fe_{0.5}^{3+}Sn^{4+}S_4$.

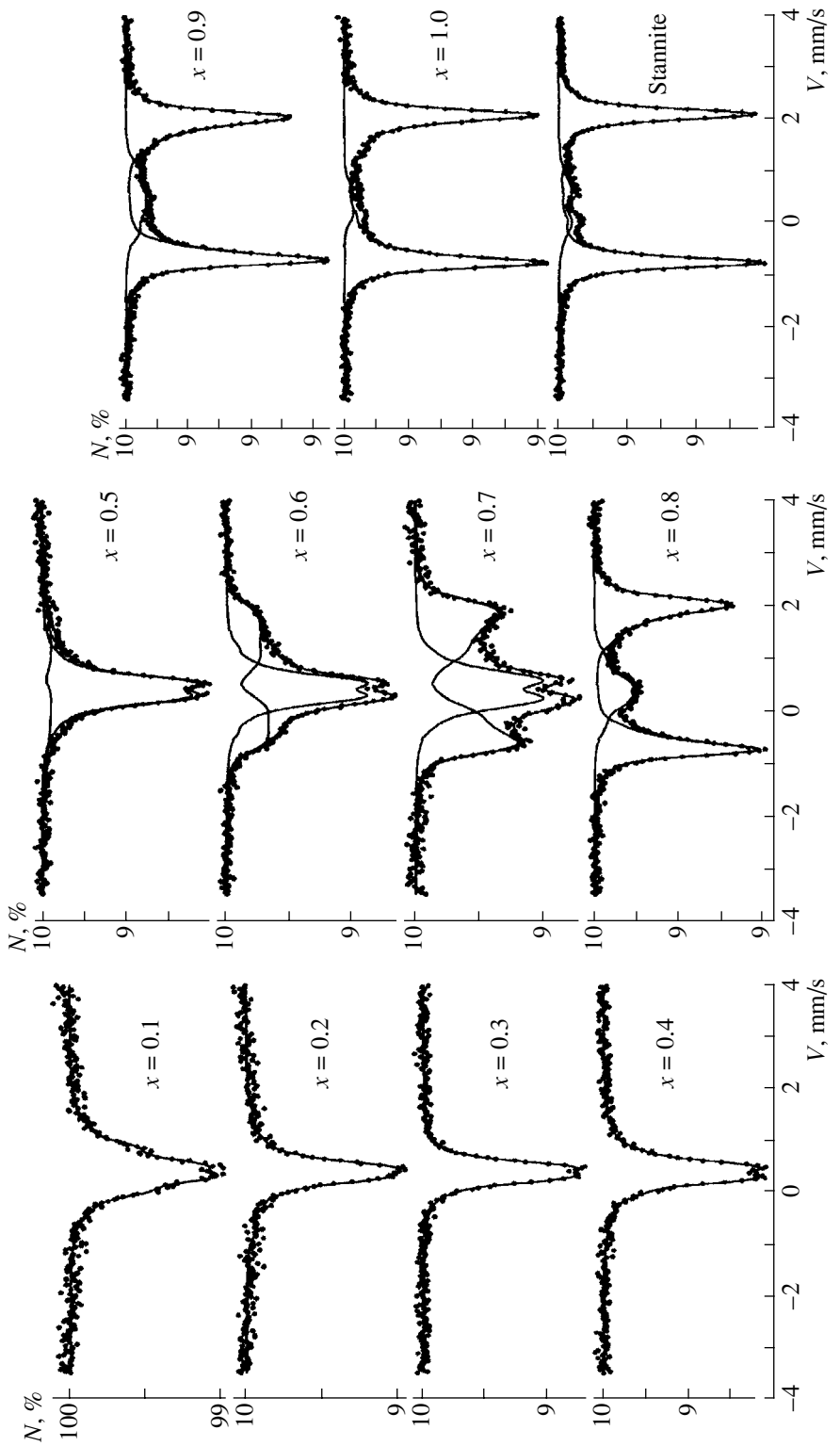

Fig. 2. Typical ^{57}Fe Mössbauer spectra of compounds of the $Cu_{3-x}Fe_xSnS_4$ series.

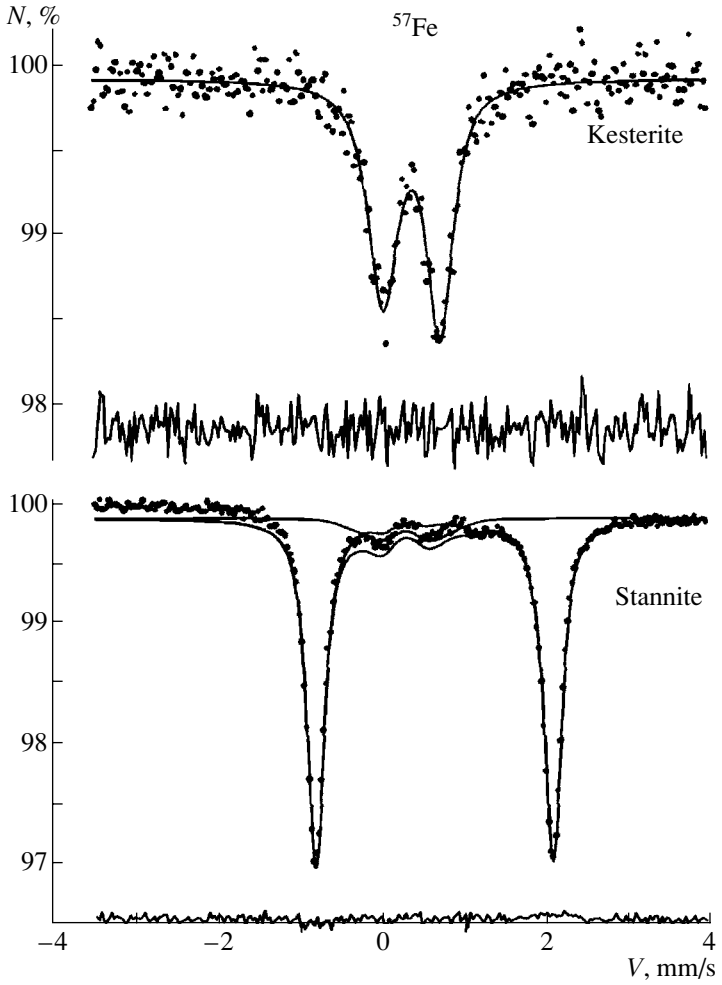

Fig. 3. ^{57}Fe Mössbauer spectra of kesterite and stannite.

The scheme of isomorphism changes above the limiting concentration $x = 0.5$:

$$Cu^{+}(Td) + Fe^{3+}(Oh) + \square(Td) \longrightarrow 2Fe^{2+}(Td),$$

with the end member $Cu_2^{1+}Fe^{2+}Sn^{4+}S_4$ forming in this process.

Indirect support for the feasibility of such a mechanism of isomorphism is provided by the results of X-ray photoelectron spectroscopy: the content of divalent copper decreases relative to that of monovalent copper with increasing iron content in the compounds of the series.

KESTERITE–STANNITE SYSTEM

The same variety of methods (EPMA, XRDA, and Mössbauer spectroscopy) was used for the investigation of kesterite with minor iron contents, $Cu_{2.00–2.03}(Zn_{0.81–0.83}Fe_{0.18})Sn_{1.00–1.03}S_{3.99–3.94}$. The analysis of Mössbauer spectra (Fig. 3) suggests the presence of ferric iron (high-spin state) in octahedral coordination by sulfur atoms (Rusakov *et al.*, 2001). The ^{57}Fe Mössbauer spectrum is somewhat asymmetric (Fig. 3). The isomer shift is 0.361(9) mm/s relative to α-Fe, and the quadrupole splitting is 0.346(9) mm/s, which is characteristic of Fe^{3+}. This is in conflict with the results of the structural analysis of kesterite, which implied substitution of iron for zinc in the tetrahedral positions (Szymanski, 1978), but agrees with the scheme of isomorphic substitutions for iron-poor members of the Cu_3SnS_4–Cu_2FeSnS_4 isomorphic series. The isomer shift of the ^{119}Sn Mössbauer line [0.012(3) mm/s relative to $BaSnO_3$ and SnO_2] and the quadrupole splitting [0.283(3) mm/s] (Fig. 4) suggest that Sn^{4+} in kesterite is tetrahedrally coordinated by sulfur atoms.

On the basis of these data, the following scheme of isomorphism with the emptying of the tetrahedral positions in the structure was proposed: $Cu^{1+} + 2Zn^{2+}(Td) \longrightarrow Cu^{2+} + \square(Td) + Fe^{3+}(Oh)$. The corresponding formula of the intermediate phases is $Cu_{2-x}^{1+}Cu_x^{2+}Zn_{1-2x}Fe_x^{3+}Sn^{4+}S_4$ (Evstigneeva *et al.*, 2003).

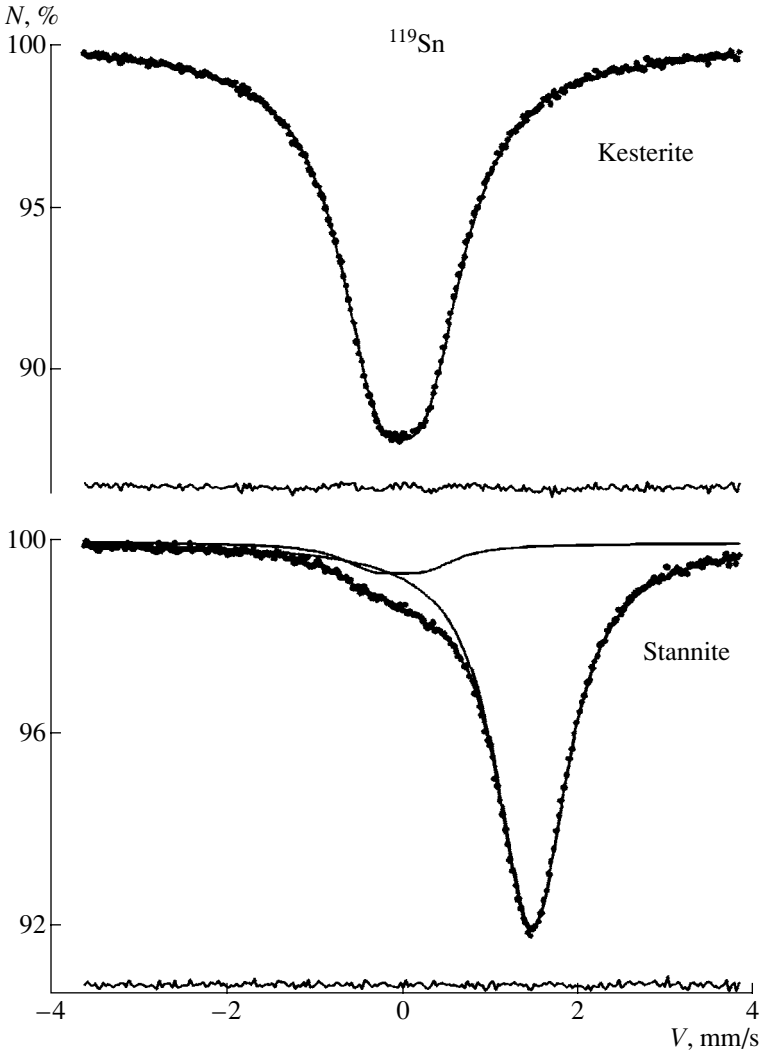

Fig. 4. ^{119}Sn Mössbauer spectra of kesterite and stannite.

THE NATURE OF "EXSOLUTION TEXTURES"

Emulsion-like chalcopyrite inclusions in sphalerite and skeletal sphalerite crystals in chalcopyrite have long been regarded as products of solid-solution unmixing (Schneiderhöhn, 1922; Betekhtin *et al.*, 1958; Ramdohr, 1975). Thermal investigations of these intergrowths showed that chalcopyrite inclusions begin dissolving in sphalerite at 400°C (Buerger, 1934) and completely disappear at 700°C (Sugaki and Yamae, 1952). Experimental studies of phase relationships in the Cu–Fe–Zn–S system (Hutchison and Scott, 1981; Kojima and Sugaki, 1985; Wiggins and Craig, 1980) revealed limited copper solubility in sphalerite and zinc solubility in chalcopyrite at temperatures of 300–400°C, at which hydrothermal sulfide ores were most likely deposited. The considerable concentrations of chalcopyrite inclusions occurring in sphalerite could not be exsolved from the high-temperature solid solution $CuFeS_2$–ZnS at decreasing temperature. This allowed a number of researchers to question the hypothesis on the formation of sphalerite–chalcopyrite intergrowths through solid solution unmixing upon cooling (Barton and Bethke, 1987; Bortnikov *et al.*, 1991; Sugaki *et al.*, 1987).

Sugaki *et al.* (1987) showed, from modal and electron microprobe analysis of chalcopyrite–sphalerite intergrowths, that the content of copper in sphalerite containing emulsion-like chalcopyrite (1.5–6.6 at. %) was higher than the solubility limit of copper in the sphalerite solid solution.

Barton and Bethke (1987) concluded that emulsion-like chalcopyrite inclusions in sphalerite were formed when earlier iron-bearing sphalerite was replaced by an aggregate of chalcopyrite and sphalerite with lower iron content.

Bortnikov *et al.* (1991) documented a diversity of sizes, forms, and distribution types of emulsion chalcopyrite inclusions in sphalerite. Tiny chalcopyrite

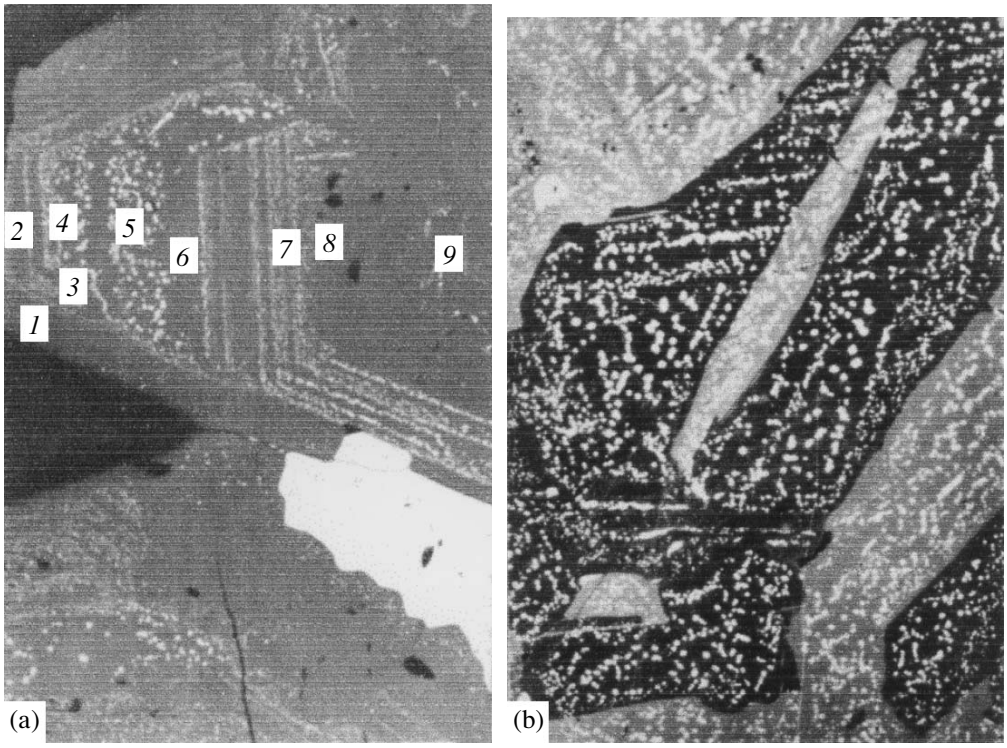

Fig. 5. Inclusions of chalcopyrite in sphalerite. (a) Zonal distribution of chalcopyrite inclusions (white) in sphalerite (gray). Black areas are quartz, and (*1–9*) are points of analysis. Sovetskii Rudnik deposit, polished section, magnification ×100 (Bortnikov *et al.*, 1991). (b) Chaotic and regular (along cleavage) distribution of chalcopyrite inclusions (white) in sphalerite (gray and black). Chernskoe deposit, polished section etched in aqua regia vapor, magnification ×100 (Bortnikov *et al.*, 1991).

inclusions in sphalerite grains are distributed nonuniformly and chaotically, forming loops, spots, and individual grains, as well as regularly along twin boundaries, fractures, cleavage planes, and growth zones.

The analysis of the chemical composition of zonal sphalerite (Fig. 5a) showed virtually identical iron contents (of 3.0–4.5 wt %) in the zones free of inclusions and in the zones with abundant chalcopyrite inclusions. The concentration of iron is lower than 2–3 wt % in the marginal zone near the sphalerite–carbonate interface. The stable chemical composition of sphalerite suggests that the appearance of chalcopyrite was not accompanied by changes in sphalerite chemistry. The absence of textural evidence for the replacement of sphalerite by chalcopyrite and the chemical homogeneity of sphalerite indicate that the zonal distribution of chalcopyrite in sphalerite was generated by the cocrystallization of these sulfides rather than through the replacement of zones composed of iron-rich sphalerite, as was supposed by Barton and Bethke (1987).

An interesting case is that of iron-rich sphalerite (13.0–14.5 wt %) containing abundant chalcopyrite inclusions in some areas and devoid of such inclusions in other zones. There exist inclusions of irregular shapes forming trails along fractures, which are sometimes parallel to each other. They associate with inclusions randomly distributed in sphalerite. It is known that the formation of exsolution textures may be accompanied by the coalescence of separate grains and development of coarser grained aggregates or veinlets. However, in such a case, the number of inclusions diminishes and the matrix is “refined” from the newly formed mineral (Brett, 1964). This phenomenon was not observed in the sample under investigation. Therefore, the observed relationships could suggest that the chalcopyrite inclusions crystallized later than the host sphalerite, in which the iron content does not change.

Some samples did not bear evidence of the confinement of chalcopyrite inclusions to grain boundaries and twin boundaries. Usually, they are randomly distributed within sphalerite grains and only occasionally show preferred orientation in two directions (Fig. 5b). Such textural relationships suggest that the chalcopyrite inclusions were formed simultaneously with sphalerite crystallization. The investigation of sphalerite chemistry in such samples (Fig. 6a) revealed variations in its composition. The outer part of grains free of chalcopyrite inclusions (Fig. 6a, I) is richest in iron (5.8–9.2 wt % Fe). The following part of grains is also free of inclusions (between the marginal zone and the zone containing inclusions), but its iron content is much lower, from 3.7 to 2.7 wt % (Fig. 6a, II). The sphalerite zones with chalcopyrite inclusions contain from 3.1 to 5.5 wt % iron (Fig. 6a, III). It is clear that the chalcopyrite–sphalerite core was formed through the cocrystallization of both sulfides. The intermediate and outer zones were formed

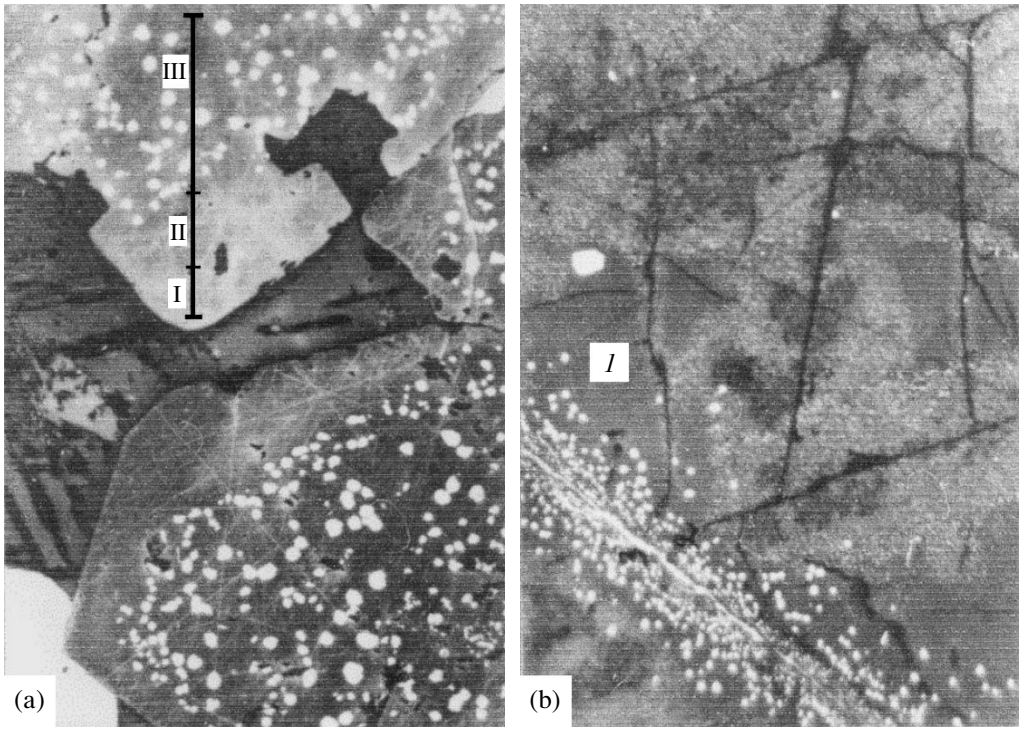

Fig. 6. Inclusions of chalcopyrite in sphalerite. (a) Irregular chaotic distribution of chalcopyrite inclusions (light) in sphalerite (gray); the outer zone on the left is a sphalerite "crust" free of inclusions, the inner part is sphalerite with chalcopyrite inclusions ("seeds"), and I–III are the sphalerite areas with different iron contents (see text). Cherninskoe deposit, polished section etched in aqua regia vapor, magnification ×100 (Bortnikov *et al.*, 1991). (b) "Islet" intergrowth texture resulting from the confinement of dustlike chalcopyrite inclusions (light) to fractures in sphalerite (gray); (*1*) and dark gray areas are porous sphalerite. Kirtisho deposit, polished section, magnification ×100 (Bortnikov *et al.*, 1991).

subsequently, and their compositions reflect variations in the contents of iron and copper in mineral-forming solutions.

In samples from some deposits, small emulsion-like inclusions are unevenly distributed, forming clusters in the form of loops, spots, and trails. The majority of relatively large and dustlike chalcopyrite inclusions are randomly distributed in sphalerite. Veinlets of late chalcopyrite, which are related to the formation of larger chalcopyrite inclusions near twin boundaries, and transformation of sphalerite, manifested in the formation of thin pressure-induced twins, support the formation of chalcopyrite inclusions through sphalerite replacement. Investigation of the chemical composition revealed 1.6–2.0 wt % of iron in sphalerite with and without chalcopyrite inclusions. The iron content of sphalerite is also invariant with the distance from contact with chalcopyrite inclusions. Thus, the formation of chalcopyrite required the input of not only Cu, but also Fe.

Sometimes (Fig. 6b), chalcopyrite inclusions trace thin fractures and veinlets in sphalerite. The emulsion-like chalcopyrite inclusions along veinlets are coarser. When chalcopyrite–sphalerite aggregates are intersected by tetrahedrite veinlets, chalcopyrite inclusions become coarser. These observations unequivocally indicate the replacement of sphalerite by chalcopyrite. Inclusion-free sphalerite contains up to 12.3 wt % Fe. Among relatively large inclusions, Fe concentration declines gradually to 9.7 wt % upon approach to a chalcopyrite veinlet. Near the veinlet, sphalerite, which has abundant dustlike inclusions, contains 5.7 wt % Fe. In this case, sphalerite replacement occurred with the addition of copper, while iron was supplied by sphalerite. In this case, both chemical and textural evidence was found for the formation of chalcopyrite inclusions at the expense of sphalerite replacement.

The characteristic features of the distribution of chalcopyrite inclusions in sphalerite and their morphology and size are difficult to explain within the exsolution model of phase crystallization (Nakano, 1937; Brett, 1964). The observed variations in the distribution density of chalcopyrite inclusions and the coexistence of areas containing abundant tiny inclusions with chalcopyrite-free zones cannot be explained by some characteristic features of the process of chalcopyrite crystallization upon the decomposition of a hypothetical high-temperature copper-bearing sphalerite. In this case, the "refinement" of sphalerite must result in the coarsening of chalcopyrite particles and formation of xenomorphic textures. The change in the morphology of chalcopyrite inclusions could have been caused by transition from coherent to incoherent unmixing owing to an increase

in the rate of exsolution and differences between the crystal structures of the newly formed minerals (Brett, 1964). In such a case, a relationship must be observed between the morphology, size, and distribution density of inclusions of newly crystallized chalcopyrite, if it was formed as a result of exsolution. However, no such connection was found in the samples studied.

Therefore, the observed chalcopyrite–sphalerite intergrowths are interpreted as a result of either simultaneous crystallization of the two minerals, or replacement of sphalerite by chalcopyrite (Barton and Bethke, 1987; Bortnikov *et al*., 1991; Bente and Doering, 1993).

The detailed investigation of regular intergrowth patterns of chalcopyrite and sphalerite has led us to the conclusion that they were formed in different ways.

(1) In some deposits, the textures of emulsion-like and dustlike chalcopyrite inclusions in sphalerite resulted from the simultaneous crystallization of sulfides from hydrothermal solutions rather than from the decomposition of solid solutions. This implies that these textures are primary and did not appear in the course of retrograde processes after ore deposition, for instance, in response to a decrease in temperature.

(2) In some deposits, chalcopyrite inclusions were formed as a result of interaction between the host sphalerite and late hydrothermal solutions. The investigation of the mineral chemistry of sphalerite suggests that the replacement of sphalerite by chalcopyrite was accompanied by the exchange of components with a mineral-forming solution: zinc was removed from the sphalerite and all or part of iron was taken for the formation of chalcopyrite. During this process, single-mineral sphalerite aggregates were replaced by the two-mineral sphalerite–chalcopyrite association.

(3) Irrespective of the mechanism of formation, the disseminated chalcopyrite is coeval with sphalerite. The selective dissolution of sphalerite with the removal of zinc implies that the mineral-forming solution is undersaturated with respect to this mineral. However, the deposition of sphalerite of a different composition and chalcopyrite indicates the supersaturation of the solution with respect to these phases. Consequently, the formation of inclusions in sphalerite suggests that the reactions of dissolution and precipitation were reversible and the sphalerite–chalcopyrite association was formed under equilibrium conditions.

Skeletal sphalerite grains in chalcopyrite have been regarded as being exsolved from the chalcopyrite solid solution (Betekhtin *et al.*, 1958; Ramdohr, 1975). Bortnikov and A.D. Genkin (1990, personal communication) noticed that star-shaped sphalerite inclusions in chalcopyrite are distributed mostly randomly and very rarely regularly. The later formation of chalcopyrite relative to sphalerite is suggested by the existence of large and small chalcopyrite veinlets emanating from aggregates in sphalerite, inclusions of chalcopyrite in sphalerite regularly arranged along veinlets, and sphalerite inclusions in large chalcopyrite and pyrrhotite grains. The sphalerite inclusions have various morphologies: skeletal sphalerite crystals show an hourglass shape (Fig. 7a); three-pointed simple and complex stars (Figs. 7b, 7c), quadratic and cross-shaped grains, and combinations of these features were observed (Figs. 7c, 7d). The sphalerite inclusions show three types of regular alignment relative to chalcopyrite. The first type is characteristic of chalcopyrite sections parallel to the (110) plane; the second, of sections parallel to (112); and the third, of sections parallel to (100). Nonuniform and occasional regular distribution of skeletal sphalerite inclusions was observed in chalcopyrite. Chalcopyrite zones free of such inclusions adjoin zones containing abundant sphalerite inclusions, which are sometimes oriented in a single direction. Characteristic features of the intergrowths of sphalerite stars with chalcopyrite are nonuniform, often irregular distribution and no preferential concentration of stars along grain and twin boundaries of the matrix. These features are different from the textures formed by exsolution, when exsolved phases are regularly distributed in the volume and sections of the host mineral (Brett, 1964). Variations in the size and morphology of stars are not correlated with the distribution density of sphalerite inclusions in chalcopyrite. The coarsening of grains of a "guest" mineral crystallizing from a solid solution occurs through the coalescence of previously formed crystals. This process results in matrix "refinement" and a decrease in the distribution density of inclusions. In the samples studied, no relationship was observed between the morphology of sphalerite stars and their distribution density in chalcopyrite.

The same features of sphalerite–chalcopyrite intergrowths were reported by Marignac (1989). This allows us to suppose that, in the deposits studied by this author, sphalerite stars were not exsolved from a solid solution during cooling.

The electron microprobe analysis of star-shaped sphalerite inclusions and coexisting chalcopyrite showed that the sphalerite contains 0.9–3.8 at. % Cu. These concentrations are higher than the values (no higher than 0.9 at. %) established for sphalerite in equilibrium with chalcopyrite at temperatures of 300–500°C (Kojima and Sugaki, 1985). Chalcopyrite with sphalerite stars contains 0.08–0.13 at. % Zn. It is known that Zn solubility in chalcopyrite in equilibrium with sphalerite increases from 0.6 at. % at 300°C to 0.9 at. % at 500°C (Kojima and Sugaki, 1985). Consequently, the concentrations of isomorphic components in coexisting minerals are not consistent with the hypothesis of the formation of skeletal sphalerite crystals through exsolution from the chalcopyrite solid solution.

Sugaki *et al.* (1987) concluded from the results of modal and electron microprobe analysis that the majority of measured bulk Zn contents in chalcopyrite with skeletal sphalerite inclusions are lower than 0.8 at. %, which corresponds to the maximum zinc solubility in chalcopyrite at 400°C. Higher Zn contents (1.2–1.4 at. %)

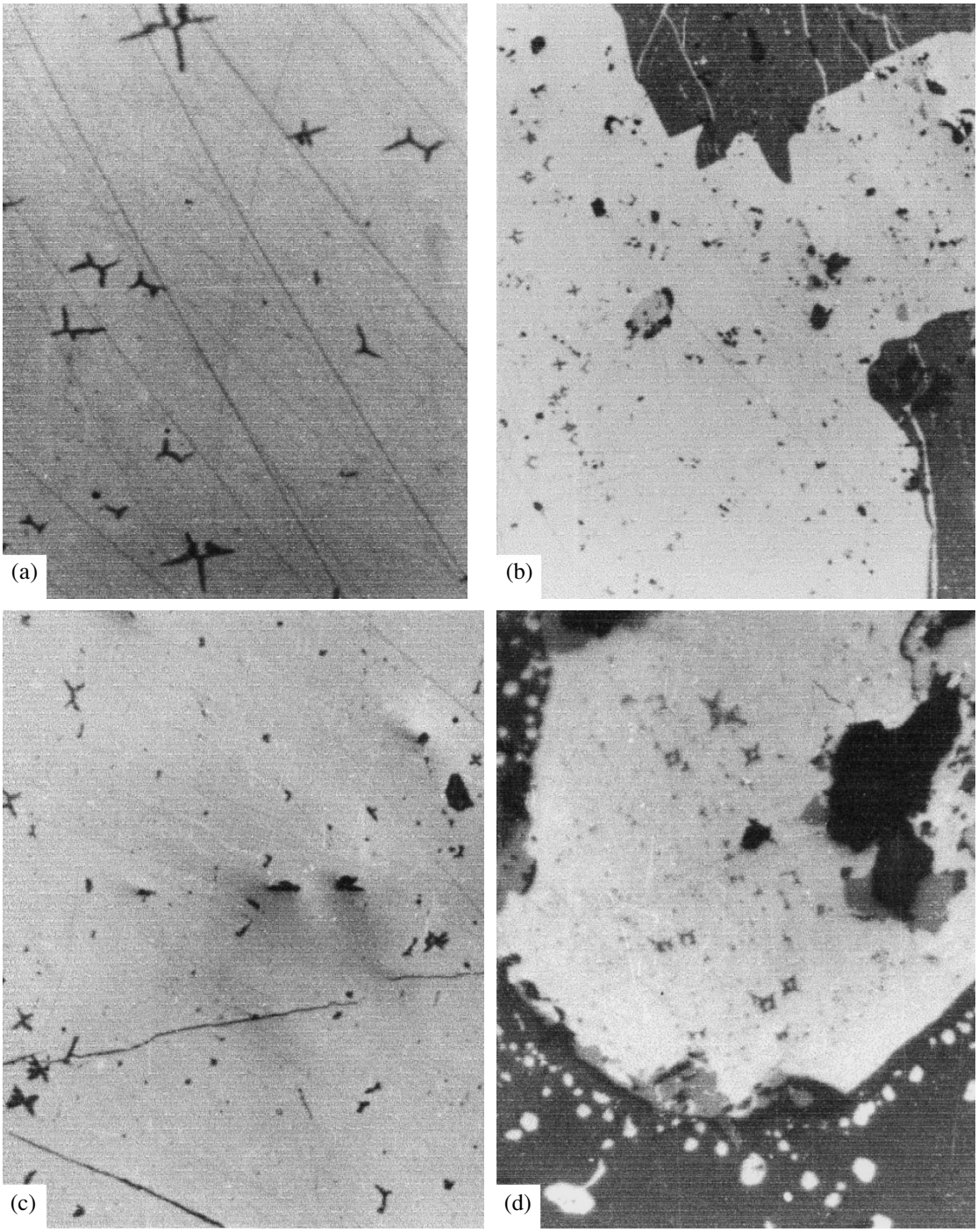

Fig. 7. Skeletal and star sphalerite inclusions (gray) in chalcopyrite (light). Polished sections, magnifications of (a–c) ×100 and (d) ×200. (a) Deputatskoe deposit; (b) Nikolaevskoe deposit; (c) Tur'inskoe deposit; and (d) Darasun deposit; chalcopyrite with sphalerite inclusions associates with sphalerite containing abundant chalcopyrite inclusions; smooth boundaries between aggregates suggest approximately simultaneous crystallization of both minerals.

in chalcopyrite from some deposits correspond to the maximum zinc solubility in Iss at temperatures higher than 400°C. This was used as a basis for the suggestion that the skeletal inclusions of sphalerite in chalcopyrite were exsolved from the chalcopyrite solid solution and/or Zn-bearing Iss.

Marignac (1989) noticed a variable spatial density of the distribution of skeletal sphalerite inclusions in chalcopyrite and the presence of their clusters. The zones of high distribution density of skeletal sphalerite inclusions contain from 0.9 to 2.6 at. % zinc, which is much higher than the experimentally determined maxi-

mum zinc content at 300°C (the temperature of sphalerite formation). This author believed that the skeletal sphalerite crystals were formed at the front of chalcopyrite growth as a result of solution supersaturation with respect to sphalerite. Thus, in his opinion, the sphalerite and chalcopyrite crystallized simultaneously.

According to Bonev (1974), the skeletal growth of sphalerite occurs in a solid medium and sphalerite nucleates at defect areas (dislocations) functioning as diffusion channels supplying zinc ions to previously formed nuclei. In the ores of the Madan region, he documented sphalerite inclusions in chalcopyrite crystals occurring in close spatial proximity with later sphalerite, which overgrows them epitaxially.

The results presented here allow the following conclusions to be made:

(1) Sphalerite stars in chalcopyrite are not exsolution products, and, similar to the emulsion-like inclusions of chalcopyrite in sphalerite, these intergrowth textures cannot be regarded as evidence for the initial precipitation of ores at high temperatures.

(2) Sphalerite stars in chalcopyrite crystallized from a hydrothermal solution after chalcopyrite formation.

(3) Variations in the chemical compositions of sphalerite of various generations suggest that the formation of sphalerite stars occurred under conditions close to undersaturation with respect to the early sphalerite generation (dissolution) and supersaturation with respect to crystallizing chalcopyrite–sphalerite aggregates. This can be considered as evidence for dynamic equilibrium during the deposition of this mineral association.

STABILITY OF MINERALS IN THE Cu–Fe–S SYSTEM

The chalcopyrite group comprises minerals of similar compositions and X-ray diffraction patterns: chalcopyrite ($CuFeS_2$), [$Cu_9(Fe, Ni)_8S_{16}$], mooihoekite ($Cu_9Fe_9S_{16}$), putoranite ($Cu_9Fe_9S_{16}$), and haycockite ($Cu_4Fe_5S_8$) (Filimonova *et al.*, 1974). Their structures are derived from the cubic cell of the sphalerite type. Since all these minerals except for chalcopyrite have metal : sulfur ratios greater than one, in addition to all tetrahedra pointing in the same direction, either tetrahedra of the opposite orientation or octahedra must be occupied. In the talnakhite structure (Hall and Gabe, 1972), the extra copper atom sits in the tetrahedral position. Chalcopyrite-group minerals and cubanite ($CuFe_2S_3$) are formed from a high-temperature solid solution (Iss) in the subsolidus of the Cu–Fe–S system (Yund and Kullerud, 1966; Fleet, 1971). In principle, the composition of associating minerals could be used to determine the temperature of Iss unmixing. However, all attempts to do this have failed, because natural minerals of this group always exhibit twin patterns and fine mutual intergrowths, which hinders the interpretation of analytical and X-ray diffraction data. Moreover, Evstigneeva *et al.* (2002) documented recently the occurrence of very thin (fractions of a micrometer) veinlets of copper sulfides (chalcocite type) in massive sulfide ores of the Oktyabr'skoe deposit composed of chalcopyrite-group minerals. This fact may change current concepts on the formation of ores with chalcopyrite-group minerals.

It is known (Cabri, 1973; Craig and Scott, 1974) that cubanite ($CuFe_2S_3$) can also form from the high-temperature solid solution (Iss) in the Cu–Fe–S system. There are two polymorphic modifications of cubanite: high (high-temperature) cubanite, with a disordered structure of the sphalerite type and a small cubic cell, and low (low-temperature) rhombic cubanite (Barton and Skinner, 1967). The experimental investigations of the Cu–Fe–S system showed that high cubanite is nonquenchable and unmixes at temperatures lower than 400°C. However, isocubanite is widespread in seafloor hydrothermal deposits. It often forms latticelike intergrowths with chalcopyrite, which resemble exsolution textures. Isocubanite is believed to be a high-temperature phase, because experimental studies demonstrated its crystallization above 210°C (Barton and Skinner, 1967) and the intermediate solid solution is stable in the Cu–Fe–S system up to a temperature of 300°C (Cabri, 1973; Craig and Scott, 1974). The appearance of chalcopyrite lamellae in isocubanite is usually related to the decomposition of a high-temperature solid solution at decreasing temperature. However, it is difficult to explain why the number of chalcopyrite lamellae may differ in adjacent grains and isocubanite grains with chalcopyrite lamellae coexist with homogeneous isocubanite grains. It is possible that chalcopyrite lamellae in isocubanite formed as a result of the transformation of the high-temperature intermediate solid solution under the influence of later fluid portions, which were characterized by varying activities of sulfur and copper. The reason for the widespread occurrence of isocubanite in modern sulfide systems is not yet clear. There is an opinion that this isocubanite is a metastable phase.

PARTITIONING OF ELEMENTS BETWEEN COEXISTING SULFIDES

The idea of using the characteristics of partitioning of elements between coexisting minerals for the estimation of temperature and the activities of some volatile components during ore formation appears very promising. It is especially attractive for the reconstruction of the conditions of formation of sulfides, because their opacity significantly complicates the investigation of fluid inclusions, the main method for determining the temperature–pressure conditions of mineralization.

Stannite–Sphalerite Geothermometry

Sphalerite and stannite are widespread in many deposits. They show wide iron and zinc isomorphism. The use of the sphalerite–stannite pair as a geother-

mometer is based on the experimentally established variations in iron and zinc distribution between these minerals (Nekrasov *et al.*, 1976, 1979; Nakamura and Shima, 1982). The equilibrium fractionation of these elements is described by the hypothetical reaction

$$Cu_2FeSnS_4 + ZnS = Cu_2ZnSnS_4 + FeS. \quad (1)$$

The distribution coefficient

$$K_D = (Fe/Zn)_{\text{in sphalerite}}/(Fe/Zn)_{\text{in stannite}} \quad (2)$$

is equivalent to the equilibrium constant of this reaction and is independent of the compositions of stannite and sphalerite solid solutions (Nekrasov *et al.*, 1976).

Two variants of the temperature dependence of K_D and corresponding thermometric expressions were proposed:

$$T°C = 1274/(1.174 - \log K_D) - 273 \quad (3)$$

(Nekrasov *et al.*, 1976) and

$$T°C = 2800/(3.5 - \log K_D) - 273 \quad (4)$$

(Nakamura and Shima, 1982).

The analysis of sphalerite coexisting with stannite (Bortnikov *et al.*, 1990) revealed iron contents from 2.5 wt % (4.4 mol % FeS) to 15 wt % (18.5 mol % FeS). The zinc content of the stannite also varies (from 1.0 to 7.8 wt %). However, despite the considerable variations of iron content in sphalerite and zinc content in stannite in the deposit, the compositions of these minerals remain constant or only slightly variable within individual grains and polished sections in the majority of samples.

Figure 8 shows the distribution of iron and zinc between coexisting sphalerite and stannite in a number of deposits. It is clearly seen that the distribution coefficients of iron and zinc between coexisting sphalerite and stannite may be variable in a particular deposit, but are almost constant for minerals from a single sample. In our opinion, this allows us to suggest that, at least in small volumes, equilibrium iron and zinc partitioning was attained during the crystallization of stannite and sphalerite. The temperatures of sphalerite and stannite formation varied from 150 to 275°C according to Eq. (3) and from 230 to 320°C according to Eq. (4).

Figure 9 compares our and published results of stannite–sphalerite geothermometry with temperatures obtained by investigation of fluid inclusions. It is known that the true temperatures of mineral formation are 20–100°C higher (depending on pressure and fluid salinity) than the temperatures of homogenization of fluid inclusions. The latter can be regarded, therefore, as the lower limits for the temperatures of mineral formation. It is evident that even the highest values calculated by Eq. (3) are lower than the homogenization temperatures of fluid inclusions. Thus, they cannot be accepted as the temperatures of mineral formation. In contrast, the values obtained by the Nakamura–Shima expression are compatible with the results of thermometric investigations of fluid inclusions.

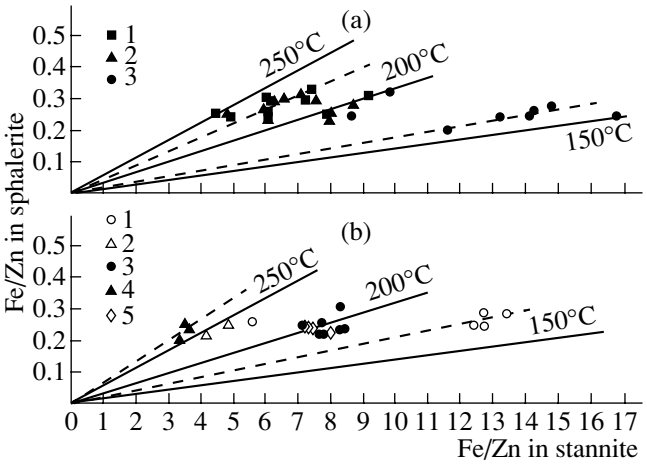

Fig. 8. Iron and zinc partitioning between coexisting sphalerite and stannite. (a) Smirnovskoe deposit: (1) Vismutovaya, (2) Povorotnaya, and (3) Glavnaya lodes. (b) (1) Lysogorskoe, (2, 3) Sinanchinskoe, and (4, 5) Dal'nee deposits; solid lines are isotherms calculated by the equation of Nekrasov *et al.* (1976), and dashed lines are isotherms inferred on the basis of analyses of various coexisting minerals (Bortnikov *et al.*, 1990).

The results of the investigation of the iron and zinc distribution between coexisting stannite and sphalerite were used for the estimation of the temperature and sulfur activity of the precipitation of these minerals (Fig. 10a). The highest sulfur activity and temperature were obtained for the formation of sphalerite–stannite ores from the base-metal skarn deposit Bokchegiano. The stannite–sphalerite aggregates from the Cinovec greisen deposit and Arsen'evskoe cassiterite–silicate deposit crystallized under similar sulfur activities and different temperatures. The formation of stannite and sphalerite occurred within a very wide temperature range in the Smirnovskoe tin–base metal deposit. It should be pointed out that, despite the relatively broad variations in temperature (225–330°C) and sulfur activity (10^{-10}–10^{-7}), the conditions of stannite and sphalerite crystallization in the majority of the objects studied fall within a narrow band in the $\log a_{S_2}$–T diagram. It is evident that sulfur activity and temperature changed in accord with the formation of aggregates of the sulfur stage of cassiterite–silicate and cassiterite–sulfide deposits. One of the processes that cause such coupled variations is fluid boiling: in this case, the removal of vapor from the system causes a decrease in temperature and H_2S evaporation reduces the activity of sulfur in the fluid. It can be supposed that this mechanism was responsible for the deposition of sulfides in the deposits considered.

An interesting regularity was observed in the deposition of stannite and sphalerite in three types of deposits: skarn, lode base-metal, and tin–tungsten (Shimizu and Shikasono, 1985) (Fig. 10b). It was found that sulfur activity increased at similar temperatures in the sequence tin–tungsten ⟶ skarn ⟶ base-metal ores.

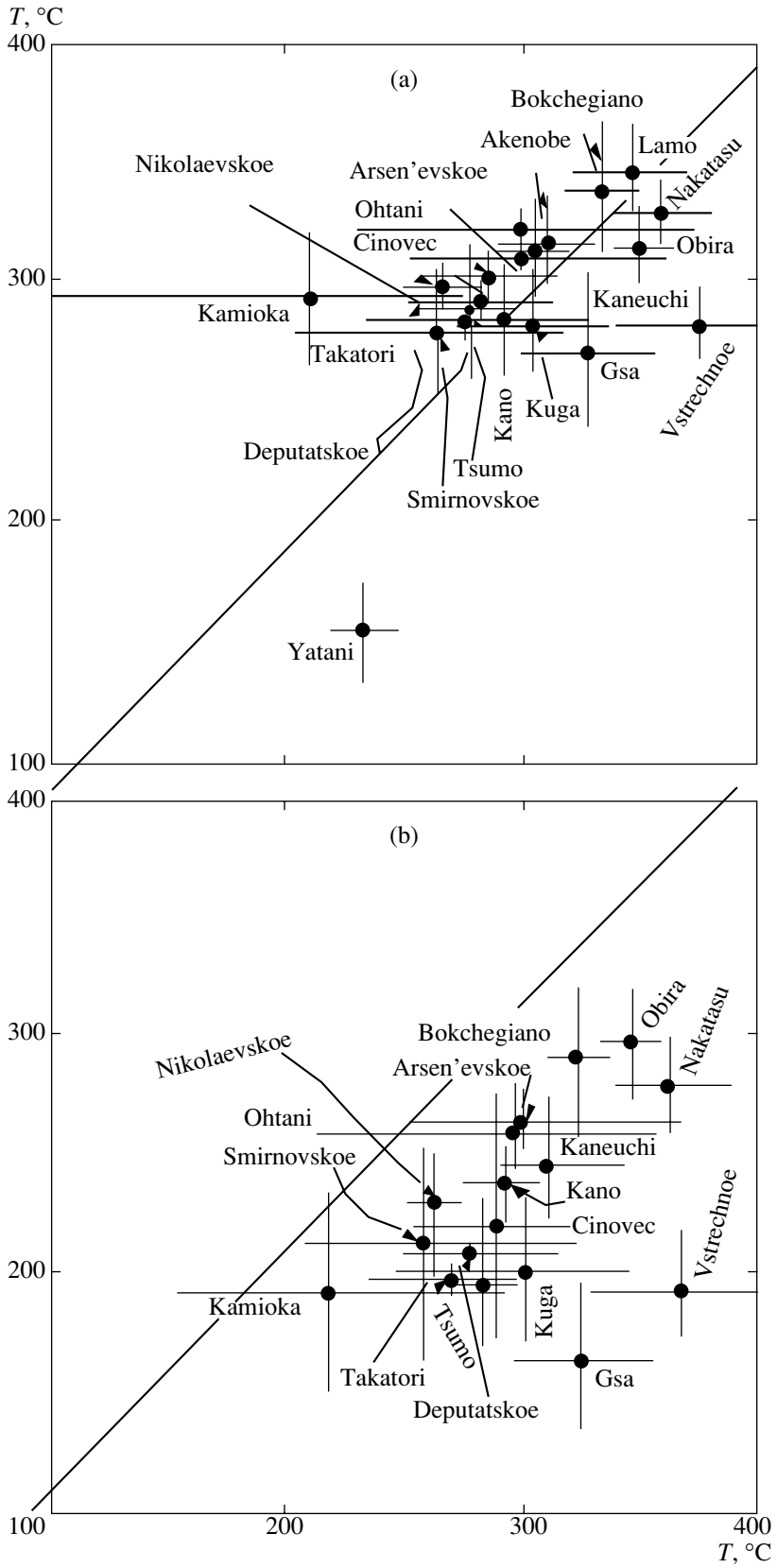

Fig. 9. Comparison of temperatures of ore formation calculated by the sphalerite–stannite geothermometer (*y* axis) with homogenization temperatures of fluid inclusions (*x* axis). Temperatures were calculated by the equations of (a) Nakamura–Shima and (b) Nekrasov *et al*. The diagram was constructed using analyses reported by Bortnikov *et al.* (1990), Simizu and Shikazono (1985), and other authors.

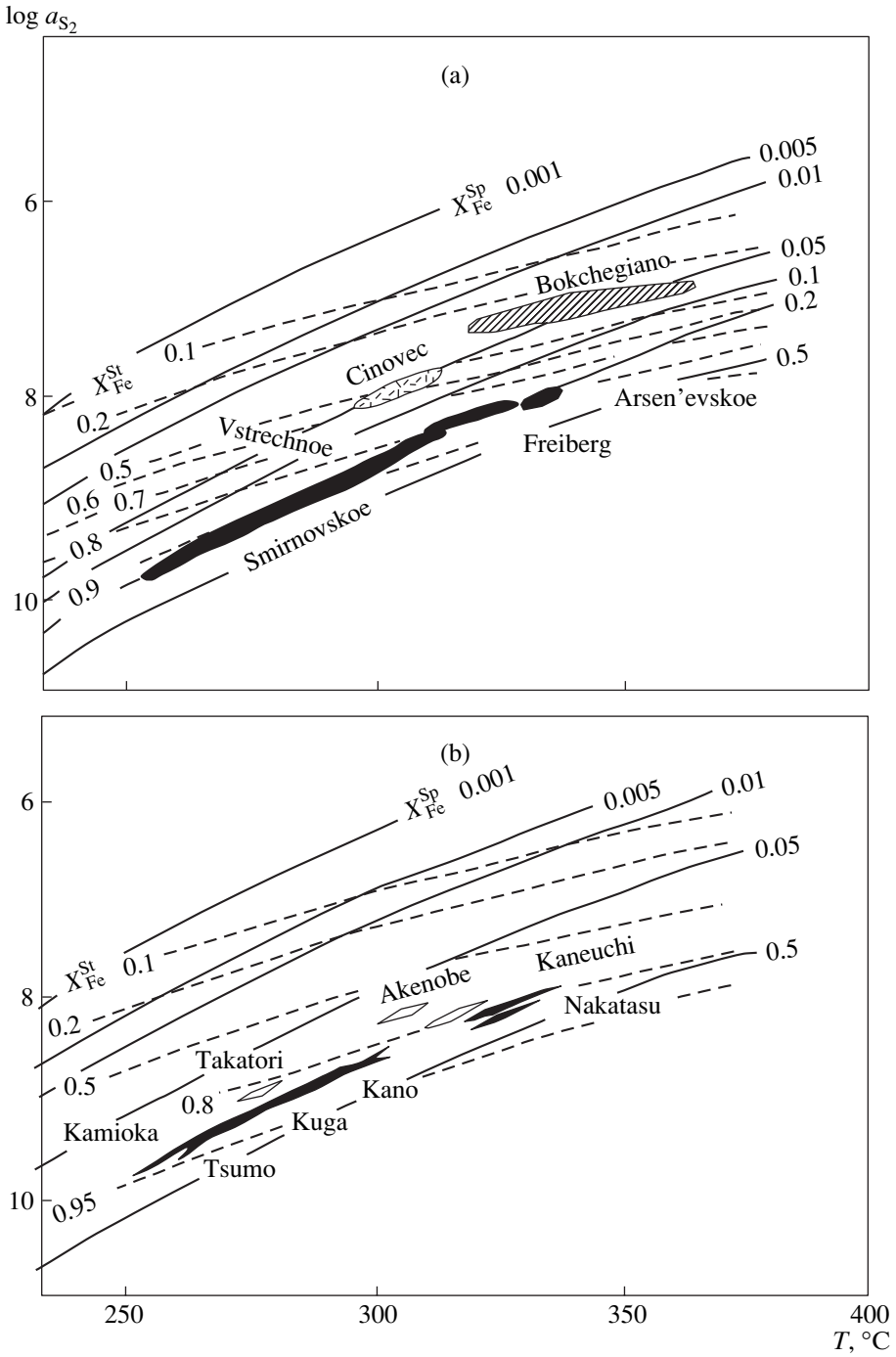

Fig. 10. Diagram showing the dependence of $\log a_{S_2}$ on temperature. The crystallization fields of stannite and sphalerite are shown.

Solid lines are isolines of the mole fraction of FeS in sphalerite (X^{SP}_{Fe}) (Scott and Barnes, 1971), and dashed lines are isolines of the mole fraction of Cu_2FeSnS_4 in stannite (Shimizu and Shikazono, 1985): (a) our data; (b) data of Shikazono with modifications. The shaded areas denote lode deposits, and the unshaded areas, skarn deposits.

Cadmium and Manganese Partitioning between Coexisting Sphalerite and Galena

Bethke and Barton (1971) and Geletii *et al.* (1979) established that the partition coefficients of CdS and MnS between coexisting galena and sphalerite depend in the PbS–ZnS–CdS and PbS–ZnS–MnS systems on temperature and pressure, and the behavior of both minerals is subject to Henry's law.

The following equations describe the influence of temperature on the partition coefficients of CdS and MnS:

$$(\log K_D)^{CdS}_{Sph\text{-}Gn} = (2080 - 0.0264P)/T - 1.8 \qquad (5)$$

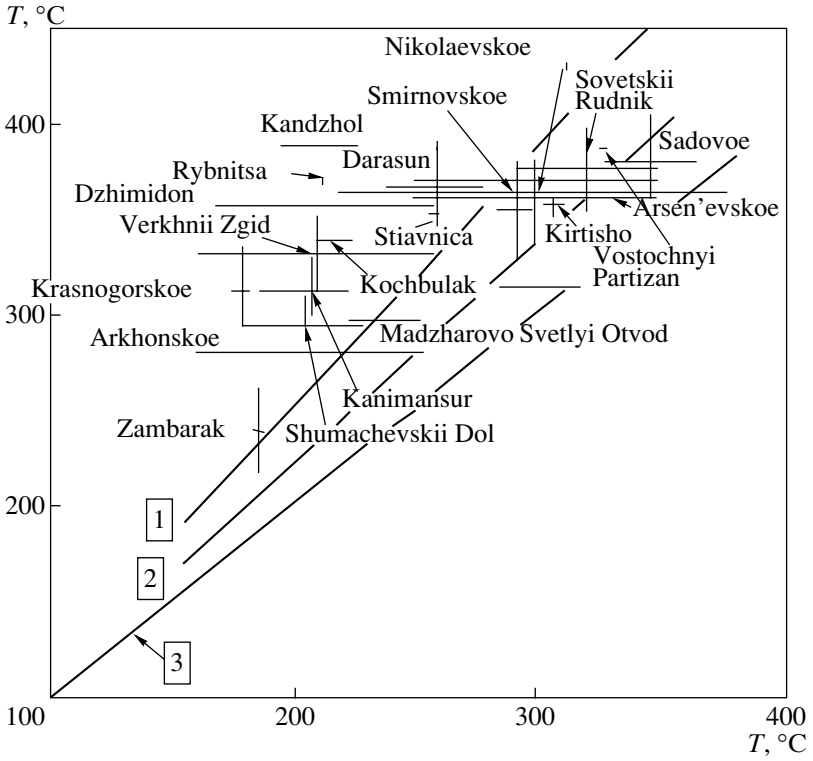

Fig. 11. Comparison of the temperatures of ore formation calculated by the sphalerite–galena cadmium geothermometer (*y* axis) with the homogenization temperatures of fluid inclusions (*x* axis). The length of the segments shows the temperature variations. Lines 1–3 correspond to pressures of (1) 1 kbar, (2) 0.5 kbar, and (3) 1 bar (Bortnikov *et al.*, 1994).

and

$$(\log K_D)^{MnS}_{Sph\text{-}Gn} = (1410 - 0.0261P)/T - 0.01. \quad (6)$$

The investigation of cadmium and manganese partitioning between coexisting sphalerite and galena showed cadmium and manganese variations in sphalerite from 0.1–2.0 and 0.0*n*–1.4 wt %, respectively. The concentrations of cadmium and manganese in galena vary from 5–60 and 4–230 ppm, respectively. The character of cadmium partitioning between coexisting sphalerite and galena in samples from a number of deposits is variable, but obeys Henry's law. Thus, it can be supposed that these minerals fulfill the conditions of equilibrium crystallization.

For the majority of samples studied, the Cd geothermometer yielded temperatures within the range 320–370°C (Fig. 11). These temperatures are 40–100°C higher than the homogenization temperatures of fluid inclusions. It can be considered that the observed departures are within the uncertainties of the two methods.

The temperatures of sphalerite and galena crystallization calculated from manganese partitioning between these sulfides vary from 61 to 737°C. In about 30% of cases, they are too high for hydrothermal ore deposits. Only a few samples yielded values comparable with the homogenization temperatures of fluid inclusions in minerals from these deposits.

In very rare cases, the temperatures estimated by the cadmium and manganese sphalerite–galena geothermometers were identical within the uncertainty of the method. There was only one case (the Arsen'evskoe deposit) when the values obtained from Cd and Mn partitioning were consistent with those deduced from the homogenization of fluid inclusions. In some cases, the temperatures of mineral formation estimated by the sphalerite–galena Mn geothermometer were compared with values calculated by the stannite–sphalerite geothermometer. It should be noted that there are discrepancies between the temperatures calculated from Cd and Mn partitioning between coexisting sphalerite and galena in single samples. Only 12 of 70 pairs analyzed showed compatible values.

The data presented here suggest that manganese partitioning between galena and sphalerite gives unreliable temperature estimates for mineral formation in many deposits and can hardly be used for geothermometry.

CONCLUSION

The general conclusion from our investigations is that the natural and experimental textures of sulfide aggregates cannot be explained on the basis of classical concepts. The character of isomorphism in ore systems indicates the block structure of mineral aggregates and their synthetic analogues. In most cases, the chemical

heterogeneity of ore minerals is caused by the presence of tiny inclusions of an additional phase or intergrowths on the micro and submicro (nano) levels. The achievements of nanomineralogy, a rapidly developing branch of mineralogy, suggest that one for the major reasons of the observed deviations of the behavior of minerals and their aggregates from the expected is the size factor. It is possible that, owing to the size factor (individuals from n to $10n$ μm), high-temperature isocubanite can be stable at low temperatures.

ACKNOWLEDGMENTS

This study was financially supported by the Russian Foundation for Basic Research, project no. 00-05-64609, and the Ministry of Industry, Science, and Technology of the Russian Federation, State Contract no. 43.016.11.1607.

REFERENCES

Barton, P.B., Jr. and Bethke, P.M., Chalcopyrite Disease in Sphalerite: Pathology and Epidemiology, *Am. Mineral.*, 1987, vol. 172, pp. 451–467.

Barton, P.B. and Skinner, B.J., Sulfide Mineral Stabilities, *Geochemistry of Hydrothermal Ore Depostis*, New York, 1967, pp. 236–333.

Bente, K. and Doering, T., Solid-State Diffusion in Sphalerites: An Experimental Verificatin of the Chalcopyrite Disease, *Eur. J. Mineral.*, 1993, vol. 5, pp. 465–478.

Bernardini, G.P., Borrini, D., Caneschi, A., Di Benedetto, F., Gatteschi, D., Ristori, S., and Romanelli, M., EPR and SQUID Magnetometyr Study of Cu_2FeSnS_4 (Stannite) and Cu_2FeSnS_4 (Kesterite), *Minerals*, 2000, vol. 27, pp. 453–461.

Betekhtin, A.G., Genkin, A.D., Filimonova, A.A., and Shadlun, T.N., *Tekstury i struktury rud* (Structures and Textures of Ores), Moscow: Gosgeoltekhizdat, 1958.

Bethke, P.M. and Barton, P., Distribution of Some Minor Elements between Coexisting Sulfide Minerals, *Econ. Geol.*, 1971, vol. 66, no. 1, pp. 140–163.

Bonev, I., Skeleton Inclusions of Sphalerite in Chalcopyrite and Their Genesis, in *Mineragenezis*, Sofiya, *Bol. Akad. Nauk*, 1974, pp. 199–200.

Bortnikov, N.S., Dobrovol'skaya, M.G., Genkin, A.D., Naumov, V.B., and Shapenko, V.V., Sphalerite-Galena Geothermometers: Distribution of Cadmium, Manganese, and Fractionation of Sulfur Isotope, *Econ. Geol.*, 1995, vol. 90, pp. 155–180.

Bortnikov, N.S., Genkin, A.D., Dobrovolskaya, M.G., Muravitskaya, G.N., and Filimonova, A.A., The Nature of Chalcopyrite Inclusions in Sphaletire: Exolution, Coprecipitation, or Disease?, *Econ. Geol.*, 1991, vol. 86, no. 5, pp. 1070–1082.

Bortnikov, N.S., Zaozerina, O.N., Genkin, A.D., and Muravitskaya, G.N., Stannite–Sphalerite Intergrowths As Possible Indicators of Ore Formation, *Geol. Rudn. Mestorozhd.*, 1990, vol. 32, no. 5, pp. 32–45.

Brett, R., Experimentall Data from the System Cu–Fe–S and Their Bearing on Exsolution Textures in Ores, *Econ. Geol.*, 1964, vol. 59, pp. 1241–1269.

Buerger, M.J., The Pyrite–Marcasite Relation, *Am. Mineral.*, 1934, vol. 19, pp. 32–61.

Cabri, L.J., New Data on Phase Relations in the Cu–Fe–S System, *Econ. Geol.*, 1973, vol. 68, pp. 443–454.

Chvileva, T.N., Bezsmertnaya, M.S., Spiridonov, E.M., *et al.*, *Spravochnik–opredelitel' rudnykh mineralov v otrazhennom svete* (Key to Ore Minerals in Reflected Light), Moscow: Nedra, 1988.

Craig, J.R. and Scott, S.D., Sulfide Phase Equilibria, *Mineral. Soc. Am. Short Course Notes*, 1974, vol. 1, pp. 1–110.

Evstigneeva, T.L. and Kabalov, Yu.A., Isomorphism of Elements in Structures of Sulfides and Intermetallic Compounds, *Tez. Pervoi Rossiiskoi Nats. kristallograf. konf.*, (Abstracts of the First Russian National Crystallographic Conference), Chernogolovka, 1998, p. 190.

Evstigneeva, T., Rusakov, V., Burkovsky, I., and Kabalov, Y., New Data on the Isomorphism Cu–Fe in Sulphides of Stannite Family, *Mineral Deposits at the Beginning of the 21st Century*, Lisse, The Netherlands, 2001a, pp. 1075–1078.

Evstigneeva, T., Rusakov, V., Kabalov, Y., Trubkin, N., Burkovsky, I., and Tschegol'kov, Y., The Complex Study of Fe–Cu Isomorphous Replacement in the Cu_3SnS_4–Cu_2FeSnS_4 Series, *Bull. Soc. Fr. Miner. Crist.*, 2001b, vol. 13, no. 3, p. 71.

Evstigneeva, T.L., Trubkin, N.V., Filimonova, A.A., Massive Cu–Ni Ores of Oktyabr'skoe Deposit of the Talnakh Ore Field, *Geologiya, genezis i voprosy osvoeniya kompleksnykh mestorozhdenii blagorodnykh metallov* (Geology, Genesis, and Problems of Development of the Precious Metal Complex Deposits), Moscow, 2002, pp. 279–283.

Evstigneeva, T.L., Rusakov, V.S., and Kabalov, Yu.K., Comparative Analysis of Isomorphic Features in Systems $Cu_{3-x}Fe_xSnS_4$ and $Cu_2Zn_{1-x}Fe_xSnS_4$, *Trudy Mineralogicheskogo muzeya* (Transactions of Mineralogical Museum) 2003 (in press).

Filimonova, A.A., Murav'eva, I.V., and Evstigneeva, T.L., Minerals of the Chalcopyrite Group in Copper-Nickel Ores of Noril'sk Deposits, *Geol. Rudn. Mestorozhd.*, 1974, vol. 17, no. 5, pp. 36–46.

Fleet, M.E., Refinement of the Crystal Sturcture of Cubanite and Polymorphism of $CuFe_2S_3$, *Z. Kristallogr.*, 1971, vol. 132, pp. 276–287.

Gamyanin, G.N., Alpatov, V.V., Bortnikov, N.S., and Anikina, E.Yu., Zonation of Silver–Base Metal Deposits, *Tez. dolk. mezhdunar. konf. "Poleznye iskopaemye: formirovanie, prognoz, resursy"* (Abstracts of Papers of Int. Conf. on Minerals Their Formation, Prospect, and Resources), St. Petersburg: Nauka, 1999, p. 125.

Geletii, V.F., Chernyshev, L.V., and Pastushkova, T.M., Distribution of Cadmium and Manganese between Galena and Sphalerite, *Geol. Rudn. Mestorozhd.*, 1979, vol. 21, no. 6, pp. 66–75.

Hall, S.R. and Gabe, E.J., The Crystal Structure of Talnakhite, $Cu_{18}Fe_{16}S_{32}$, *Am. Mineral.*, 1972, vol. 57, pp. 368–380.

Hall, S.R., Szymanski, J.T., and Stewart, J.M., Kesterite, $Cu_2(Zn, Fe)SnS_4$, and Stannite, Cu_2FeSnS_4, Strcuturally Similar But Distinct Minerals, *Can. Mineral.*, 1978, vol. 16, pp. 131–137.

Hutchinson, M.N. and Scott, S.D., Sphalerite Geobarometry in the System Cu–Fe–Zn–S, *Econ. Geol.*, 1981, vol. 76, pp. 143–155.

Kissin, S.A., A Reinvestigation of the Stannite (Cu_2FeSnS_4)–Kesterite (Cu_2ZnSnS_4), Pseudobinary System, *Can. Mineral.*, 1989, vol. 27, no. 4, pp. 689–697.

Kissin, S.A. and Owens, D.R., The Relatives of Stannite in the Light of New Data, *Can. Mineral.*, 1989, vol. 27, p. 673.

Kojima, S. and Sugaki, A., Phase Relations in the Cu–Fe–Zn–S System between 500 and 300°C under Hydrothermal Conditions, *Econ. Geol.*, 1985, vol. 80, pp. 58–171.

Kovalenker, V.A., Evstigneeva, T.L., Troneva, N.V., and Vyal'sov, L.N., Kuramite, Cu_3SnS_4, As a New Mineral of the Stannite Group, *Zap. Vses. Mineral. O–va*, 1979, part 108, no. 5, pp. 564–569.

Marignac, Ch., Sphalerite Stars in Chalcopyrite; Are They Always the Result of an Unmixing Process? *Miner. Deposita*, 1989, vol. 24, pp. 176–182.

Nakamura, Y. and Shima, H., Fe and Zn Partitioning between Sphalerite and Stannite, *Joint Meeting of Soc. Mining. Geol., Japan and Miner. Soc. Japan* (Abstract), 1982.

Nakano, N., On the Microscopic Intergrowth of Chalcopyrite and Zincblende, *J. Japan. Assoc. Mineral. Petrol., 1937, Econ. Geol*, 1940, vol. 18, pp. 23–29.

Nekrasov, I.Ya., Sorokin, V.I., and Osadchii, E.G., Fe and Zn Partitioning between Sphalerite and Stannite at T = 300–500°C and P = 1 kbar, *Dokl. Akad. Nauk SSSR*, 1976, vol. 226, no. 5, pp. 1166–1168.

Nekrasov, I.J., Sorokin, V.I., and Osadchij, E.G., Fe and Zn Partitioning between Stannite and Sphalerite and Its Application in Geothermometry, *Origin and Distribution of Elements*, New York: Pergamon, 1979, pp. 739–742.

Orlova, Z.V., Kesterite as a New Mineral, *Zap. Vses. Mineral. O–va*, 1958, part 87, no. 1, pp. 76.

Osadchii, E.G. and Sorokin, V.I., *Stanninsoderzhashchie sul'fidnye sistemy* (Stannite-Bearing Sulfide Systems), Moscow: Nauka, 1989.

Ramdohr, P., *Ore Minerals and Their Intergrowths*, New York: Springer, 1975.

Rusakov, V.S., Evstigneeva, T.L., and Burkovskii, I.A., Mössbauer Spectroscopy of Kesterite, $Cu_2(Zn, Fe)SnS_4$, *Traditsionnye i novye napravleniya v mineralogicheskikh issledovaniyakh: Tr. godichnoi ses. MO VMO* (Traditional and New Lines in Mineralogical Studies: Proceedings of Yearly Session of Moscow Division of All-Russia Minera. Soc.), Moscow: Inst. Geol. Rudn. Mestorozhd., Ross. Akad. Nauk, 2001.

Schneiderhöhn, H., *Anleitung zur microscopischen Bestimmung und Untersuchung von Erzen Und Aufbereitungsproducton, besonderes im auffalenden Licht*, Berlin, 1922.

Shimizu, M. and Shikazono, P., Iron and Zinc Partitioning between Coexisting Stannite and Sphalerite: A Possible Indicator of Temperautre and Sulfur Fugacity, *Miner. Deposita*, 1985, vol. 20, pp. 314–320.

Springer, G., The Pseudobinary System Cu_2FeSnS_4–Cu_2ZnSnS_4, and Its Mineralogical Significance, *Can. Mineral.*, 1972, vol. 11, pp. 535–541.

Sugaki, A. and Yamae, N., Thermal Study on the Intergrowth of Chalcopyrite and Sphalerite, *Sci.Rep. Togoku Univ. Ser. 3*, 1952, vol. 4, pp. 103–110.

Sugaki, A., Kitakaze, A., and Kojima, S., Bulk Compositions of Intimate Intergrowths of Chalcopyrite and Sphalerite and Their Genetic Implications, *Miner. Deposita*, 1987, vol. 22, pp. 26–32.

Szymanski, J.T., The Crystal Structure of Černyite, Cu_2CdSnS_4, a Cadmium Analogue of Stannite, *Can. Mineral.*, 1978, vol. 16, pp. 147–151.

Wiggins, L.B. and Craig, J.R., Reconnaissance of the Cu–Fe–Zn–S System: Sphalerite Phase Relations, *Econ. Geol.*, 1980, vol. 75, pp. 742–751.

Yund, R.A. and Kullerud, G., Thermal Stability of Assemblages in Cu–Fe–S System, *J. Petrol.*, 1966, vol. 7, pp. 454–488.